

# Absorption Cross-Section and Near-Field Enhancement in Finite-Length Carbon Nanotubes in the Terahertz-to-Optical Range

M. V. Shuba\*, S. A. Maksimenko and G. Ya. Slepyan,

*Institute for Nuclear Problems, Belarus State University, Bobruiskaya 11, 220050 Minsk, Belarus*

Electromagnetic characteristics of single-walled finite-length carbon nanotubes – absorption cross-section and field enhancement in the near zone – are theoretically studied in a wide frequency range from terahertz to visible. The analysis is based on the impedance-type effective boundary conditions and the integral equation technique. Comparison with experimental results is carried out allowing qualitative physical interpretation of low-frequency (far-IR and terahertz) absorption band observed in experiments. Potentiality of CNTs for the IR photothermolysis of living cells is discussed. Strong local field enhancement is predicted to be inherent to metallic CNTs in the near-field zone providing necessary mechanism for far-IR and terahertz near-field optics.

**Keywords:** Carbon Nanotube, Absorption Cross-Section, Near-Field Enhancement.

PACS numbers: 42.70.-a, 73.25.+i, 77.84.Lf, 78.67.Ch

## I. INTRODUCTION

Promising potentiality of nano-scale objects and nano-structured systems for transmission and processing electromagnetic signals motivates active and permanently growing investments into studying their electromagnetic response. A new branch of physics of nanostructures nanoelectromagnetics is currently emerging. Among others, carbon nanotubes<sup>1</sup> (CNTs) are of special interest owing their unusual electronic and mechanical properties, temperature stability and quasi-one-dimensional nature. Single-walled CNTs are hexagonal networks of carbon atom rolled up into cylinder  $\sim 1 - 3$  nm in diameter and  $\sim 0.1 - 10$   $\mu$ m in length. Recently, CNTs were proposed for realization of different integrated circuits elements and electromagnetic devices, such as transmission lines<sup>2,3,4,5</sup>, interconnectors<sup>6,7,8,9,10</sup> and nanoantennas<sup>11,12,13,14,15,16,17,18,19,20,21</sup>. First experimental realization of the CNT-based radio have been reported<sup>22,23</sup> and potentiality of CNTs as terahertz and infrared light emitters has been demonstrated<sup>24,25,26,27,28,29,30</sup>. Strong absorbance of CNTs in optical and terahertz ranges<sup>31,32,33,34,35</sup> can be used for electromagnetic stimulation of nanotubes inside living cells to afford various useful functions<sup>36</sup> and, in particular, for the selective cancer photothermolysis<sup>36,37,38,39</sup>. Note that the plasmonic photothermal therapy using gold nanoparticles has emerged to be highly promising for cancer therapy and is fast developing<sup>40,41,42</sup>.

Obviously, the nanophotothermal effect is expected to be efficient only in the maximal-absorption band whether it be the plasmon resonance in metal nanoparticles or geometrical (antenna) resonance<sup>14</sup> in CNTs. As different from the plasmon, the antenna operating frequency is dic-

tated by the CNT length and therefore provides spectral tunability of the method. Moreover, the strong slowing-down effect characteristic for the surface wave propagation in CNTs<sup>2</sup> shifts geometrical resonances to the red opening far-infrared and terahertz ranges for the nanothermolysis. Although water is opaque in the terahertz range preventing most living cells from the CNT-based terahertz photothermal therapy, the method can be useful for tissue with low water content, e.g. fatty tissue. Of course, elaboration of a consistent theory of the CNT-based photothermolysis of living cells is a global scientific problem comprising many physical, chemical and biological subtasks. Among others, the heat transfer between CNT and fluidic cell volume is of special interest, first of all because it is governed by specific thermodynamics of CNTs. It should be emphasized that the nanothermodynamics as a whole<sup>43,44</sup> and, in particular, the thermodynamics of CNTs<sup>45,46,47,48</sup> essentially differ from the classical macroscopic thermodynamics. However, even so, the absorption cross-section  $\Lambda(\lambda)$ , where  $\lambda$  is the wavelength, remains to be a basic quantity defining exterior heat source in the cell.

That is why theoretical prediction of spectral properties of the CNT absorption cross-section  $\Lambda(\lambda)$  is a critical problem for many medical and electromagnetic applications of CNTs. In our paper we present a theory of electromagnetic wave absorption by finite-length carbon nanotubes in a wide spectral range from terahertz to visible frequencies. The theory allow correct interpretation of experimental results reported in Refs.<sup>32,33,34,35</sup> – a resonant behavior of dielectric properties of single-walled CNT film in terahertz and infrared regimes. Explanations of the behavior by the phonon resonance<sup>35,49</sup> or energy gap due to the CNT curvature<sup>50</sup> do not respond the question properly. Indeed, as was mentioned by Bommeli *et al.*<sup>32</sup>, the far-infrared (terahertz) absorption resonance is temperature independent and therefore can not be related to phonon modes. Moreover, the absorption peak shifts in frequency when measuring different specimens, and consequently cannot be strictly con-

---

\*Author to whom correspondence should be addressed: Tel.: +37517 2264220; fax: +37517 2265124. *E-mail address:* mikhail.shuba@gmail.com.

sidered as an intrinsic properties of the nanotubes like a phonon mode. This is reasonable argumentation against the phonon model. As for the second explanation, no direct calculations of the curvature impact on the scattering and absorption properties of CNTs have been provided for comparison with experimental data.

Recently, we have proposed<sup>14,17</sup> alternative explanation of the quasi-resonant behavior of dielectric properties of CNTs in terahertz and far-infrared region. We have found that owing to the strong slowing down of surface waves (plasmon-polariton modes) in CNTs<sup>2</sup>, the geometrical (antenna) resonances are shifted to the red and, for micrometer-length CNTs, appear to be in the terahertz range. This is pure finite-length electromagnetic effect which dictates the peculiarities of IR and terahertz properties of CNTs. In the present paper we utilize the finite-length CNT model combining the quantum-mechanical dynamic conductivity<sup>2</sup> and the integral equations method<sup>51</sup>, for solving the electrodynamic boundary-value problem. That allows us to give a satisfactory explanation of experimental data<sup>34</sup> for the CNT film absorbance in a wide frequency range. We also investigate the CNT ability to produce highly localized electromagnetic fields – extremely interesting property for near-field optics, realization of the Parcell effect for terahertz-range emitters and as a means for the surface plasmon excitation in metallic substrates.

## II. THEORETICAL CONSIDERATION

In theoretical analysis of electromagnetic properties of finite-length CNT we combine methods of classical electrodynamics and semiclassical physical kinetics, see Refs.<sup>2,14</sup>. The latter means that the motion of  $\pi$ -electrons in CNT is described as classical motion of quasi-particles with quantum dispersion law accounting for the hexagonal crystalline structure of graphene and quantization of the transverse momentum. This allows us to formulate effective boundary conditions for electromagnetic field on the CNT surface in the form of two-side anisotropic impedance boundary conditions<sup>2</sup>. The CNT electronic properties are incorporated into analysis by means of the surface impedance tensor. In this case the problem of the CNT-based antenna is reduced to the boundary-value problem of classical electrodynamics.

Let an isolated single-walled CNT of length  $L$  and cross sectional radius  $R$  be aligned parallel to the  $z$  axis of the cylindrical coordinate system  $(\rho, \varphi, z)$ . The origin of coordinate system is located at the point  $z = 0$  in the geometrical center of the CNT. The nanotube is exposed to external field with  $E_z^{(0)}(z, R) \exp(-i\omega t)$  as  $z$ -component;  $\omega$  is the angular frequency. This field induces in CNT axial surface current of the density  $\mathbf{j}(\mathbf{r})$ , which reradiates the scattered field. Assuming the CNT radius to be small as compared to the free-space wavelength, we neglect the transverse current in CNT. We also neglect azimuthal variations of the axial current on the CNT surface, that

is we set  $\mathbf{j}(\mathbf{r}) = j(z)\mathbf{e}_z$ , where  $\mathbf{e}_z$  is the unit vector along the CNT axis.

The electric Hertz potential of scattered field  $\Pi(\rho, z)$  satisfies the Helmholtz equation and radiation conditions, and can be represented in the form of single-layer potential<sup>14</sup>:

$$\Pi(\rho, z) = \frac{iR}{\omega} \int_{-L/2}^{L/2} j(z')G(z-z', \rho, R)dz', \quad (1)$$

where

$$G(z, \rho, R) = \int_0^{2\pi} \frac{\exp\left(ik\sqrt{\rho^2 + R^2 - 2R\rho\cos\varphi + z^2}\right)}{\sqrt{\rho^2 + R^2 - 2R\rho\cos\varphi + z^2}} d\varphi. \quad (2)$$

Imposing boundary conditions on the CNT surface<sup>2</sup> we arrive at the integral equation for the current density:

$$\begin{aligned} & \int_{-L/2}^{L/2} E_z^{(0)}(R, z')e^{ik|z-z'|} dz' + Ce^{ikz} + De^{-ikz} \\ &= \int_{-L/2}^{L/2} \left[ \frac{4\pi R}{c} G(z-z', R, R) + \frac{1}{\sigma} e^{ik|z-z'|} \right] j(z') dz', \quad (3) \end{aligned}$$

where  $\sigma$  is the CNT axial conductivity derived via quantum transport theory<sup>2</sup>, whereas  $C$  and  $D$  are unknown constants to be determined from the edge conditions

$$j(\pm L/2) = 0, \quad (4)$$

which express the absence of concentrated charges on the CNT edges  $z = \pm L/2$ .

Generally, Eq. (3) can not be solved analytically. For numerical solution the integral on the right side of (3) is numerically handled by a quadrature formula, thereby transforming Eq. (3) into a matrix equation. Solution of matrix equation gives axial current density  $j(z)$  along CNT. The spatial distribution of the non-zero component of the scattered electromagnetic field in arbitrary point can be found as follows:

$$E_\rho = \frac{\partial^2 \Pi}{\partial \rho \partial z}, \quad E_z = \left( \frac{\partial^2}{\partial z^2} + k^2 \right) \Pi, \quad H_\phi = ik \frac{\partial \Pi}{\partial \rho}. \quad (5)$$

The CNT absorption cross-section along the  $z$ -axis is determined by the relation

$$\Lambda = P_t / I_0, \quad (6)$$

where

$$P_t = \pi R \operatorname{Re} \left( \frac{1}{\sigma} \right) \int_{-L/2}^{L/2} |j(z)|^2 dz \quad (7)$$

is the power loss due to current dissipation, and  $I_0$  is the intensity of incident electromagnetic wave; for plane wave  $I_0 = (c/8\pi)|E_z^{(0)}|^2$ .

Electromagnetic characteristics of CNT demonstrate qualitatively different behavior in two fundamentally distinguishing regimes. The first one, further referred to as the Drude conductivity regime, is characterized by the propagation of low-attenuated surface waves<sup>2</sup> and corresponding geometrical resonances<sup>14</sup> in finite-length CNTs. The resonances are due to intraband motion of conducting electrons. The second one – called as the optical transitions regime – is determined by the interband transitions of electrons. In the Drude conductivity regime, CNT is analogous in many respects to macroscopic RF wire antenna<sup>7,12,13,14</sup>. Regime of optical transitions has quantum nature and, consequently, has no macroscopic analogs. The angular frequency  $\omega_e$ , which divides the Drude conductivity regime ( $\omega < \omega_e$ ) and the regime of optical transition ( $\omega > \omega_e$ ), depends on the electronic and geometric properties of concrete CNT. From the approximate relation for the density of electron states<sup>52</sup> one can find that  $\omega_e \approx 2v_F/R$  and  $\omega_e \approx 2v_F/(3R)$  for metallic and semiconducting CNT, respectively;  $v_F$  is the  $\pi$ -electron velocity at the Fermi level.

As has been shown in Refs.<sup>14,15</sup>, in the range of interband transitions the surface waves in single-walled CNTs are strongly attenuated. Therefore, the surface current density  $j(z)$  in a nanotube exposed to external electric field obeys with high accuracy the Ohm's law,

$$j(z) = \sigma E_z^{(0)}(z), \quad (8)$$

which is indeed the first Born approximation of scattering theory in application to Eq. (3).

The use of Eq. (8) as an approximate solution of the integral equation (3) is only possible when the local electric field on the CNT surface is much smaller than the external electric field, i.e. the relation

$$\left| \left( \frac{\partial^2}{\partial z^2} + k^2 \right) \Pi(R, z) \right| \ll |E_z^{(0)}(R, z)| \quad (9)$$

holds true over the CNT length.

Note that the solution (8) does not satisfy the edge conditions (4). However, the error is strongly localized in the vicinity of the edges and therefore does not influence the field formation in far-field region; analogous situation appears, for example, in the theory of diffraction by an aperture in infinitely thin perfect screen<sup>51</sup>. A comparison of the exact solution by Eq. (3) with approximate calculations by Eq. (8) shows that the latter one can serve for high-accuracy evaluation of CNT scattering and absorption parameters in the interband transition regime.

Substitution of (8) into Eqs. (7) and (6) leads to the simple formula for the absorption cross-section of isolated CNT in the interband transitions regime in the  $z$ -direction:

$$\Lambda = \frac{8\pi^2 RL}{c} \text{Re}(\sigma). \quad (10)$$

In that regime, this formula can be directly applied to calculation of the absorbance of a bundle of parallel CNTs.

As has been shown by Hao and Hanson<sup>15</sup>, in the regime of interband transitions the electromagnetic coupling of carbon nanotubes composed in a planar array is very low. Therefore, the current in an individual tube of the array can be found from (8). Extending that result to CNT bundle comprising  $N$  nanotubes, we arrive at the formula

$$\Lambda_c = \sum_{m=1}^N \Lambda_m \quad (11)$$

for the absorption cross-section of the bundle in the direction parallel to its axis. In this expression,  $\Lambda_m$  is absorption cross-section of  $m$ th CNT. Because of the strong electromagnetic coupling of metallic CNTs in the Drude conductivity regime<sup>17</sup>, in this regime the formula (11) can not be applied to bundles comprising more than one metallic CNT.

### III. NUMERICAL RESULTS

#### A. CNT absorption cross-section

Figure 1 demonstrates the normalized absorption cross-section  $\Gamma(\lambda) = \Lambda(\lambda)/(2RL)$  of (9,0) metallic zigzag CNT for different CNT lengths  $L$  and different electron mean free-path time  $\tau$ . The value  $\tau$  is used under calculation of the axial conductivity<sup>2</sup>  $\sigma$  and is assumed to be constant over the whole frequency range considered. As it is seen, three different bands are distinguished in

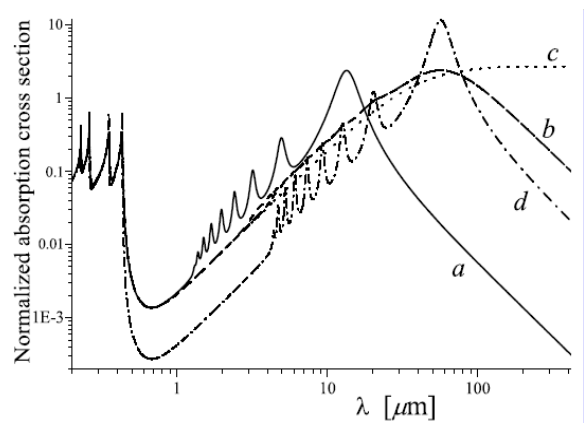


FIG. 1: Normalized absorption cross-section  $\Gamma(\lambda)$  of (9,0) zigzag CNT; *curve a*:  $L = 100$  nm,  $\tau = 2 \times 10^{-14}$  s, *curve b*:  $L = 500$  nm,  $\tau = 2 \times 10^{-14}$  s, *curve c*:  $L = 6000$  nm,  $\tau = 2 \times 10^{-14}$  s, *curve d*:  $L = 500$  nm,  $\tau = 1 \times 10^{-13}$  s.

Fig. 1, characterizing the (9,0) CNT interaction with electromagnetic field: the Drude conductivity regime ( $\lambda \gtrsim 1 \mu\text{m}$ ), the optical transitions regime ( $\lambda \lesssim 0.5 \mu\text{m}$ ), and the intermediate regime ( $0.5 < \lambda < 1 \mu\text{m}$ ).

In the regime of Drude conductivity the cross-section  $\Gamma(\lambda)$  demonstrates a set of resonances. Intensity of resonances grows smaller as wavelength decreases, whereas

the length  $L$  increase shifts the resonances to the red and leads to their broadening (compare lines  $a$  and  $b$  in Fig. 1), so that they completely disappear at sufficiently large  $L$  (see line  $c$ ). The same effect is observed with the increase of  $\tau$ , compare lines  $b$  and  $d$ , while the resonant wavelengths do not depend on  $\tau$ . Physically, the resonances depicted in Fig. 1 are the geometrical (antenna) resonances<sup>14</sup> whose wavelengths are dictated by the condition of the standing surface wave to be settled. In view of conditions (4) the resonant wavelengths are approximately determined by

$$2Lc = s\lambda_s v(\lambda_s), \quad s = 1, 3, 5, \dots, \quad (12)$$

where  $v(\lambda)$  is the surface wave phase velocity at the wavelength  $\lambda$ . It should be noted, that in the Drude conductivity regime the surface waves in CNT are strongly slowed down<sup>2</sup>:  $v(\lambda) \ll c$ . Therefore, accordingly to (12) the resonant wavelength is much longer than the CNT length:  $\lambda_s \gg L$ . For example, line  $a$  in Fig. 1 shows three first geometrical resonances of 100 nm length CNT at  $\lambda_1 = 12.7 \mu\text{m}$ ,  $\lambda_2 = 4.9 \mu\text{m}$  and  $\lambda_3 = 3.2 \mu\text{m}$ .

In the short-wavelength regime ( $\lambda < 0.5 \mu\text{m}$ ) the spectral dependence  $\Gamma(\lambda)$  also demonstrate a set of resonances, which are due to  $\pi$ -electron transitions between valence and conduction bands. Obviously, in this regime the normalized absorption cross-section does not depend on the CNT length (see Fig. 1) and is completely determined by the CNT conductivity accordingly to Eq. (10). The CNT conductivity resonances correspond<sup>2</sup> to Van-Hove singularities of the density of states of  $\pi$ -electrons.

In the intermediate region, both interband and intraband motion of  $\pi$ -electrons contribute into the CNT conductivity. Our calculations shows that in this range the quantity  $\Gamma(\lambda)$  turns out to be very small, has no resonances and practically does not depend on the CNT length (compare lines  $a$ ,  $b$  and  $c$  in Fig. 1), while demonstrates strong dependence on  $\tau$ .

## B. Comparison with experiment

The experimentally registered by Hu *et al.*<sup>34</sup> normalized absorbance  $\Lambda_c$  of a film comprising a sparse disordered array of finite-length bundles of single-walled CNTs is depicted in Fig. 2 by solid line. The plot has been extracted from Fig. 6 of cited article. In this article, the CNT bundles were found to have average diameter 2.7 nm and length  $L < 2 \mu\text{m}$ . The dashed curves in Fig. 2 show calculated absorption cross-section  $\Lambda_b$  of a bundle of three zigzag tubes (one metallic and two semiconductor CNTs) with chiral vectors (13,0), (12,0) and (11,0). The semiconductor nanotubes (13,0) and (11,0) have been chosen because their first interband transitions fit well the experimentally observed extremums in the high-frequency part of the absorption spectrum, as it is seen in Fig. 2. The low-frequency pick on the theoretical curve is completely due to geometrical resonance of

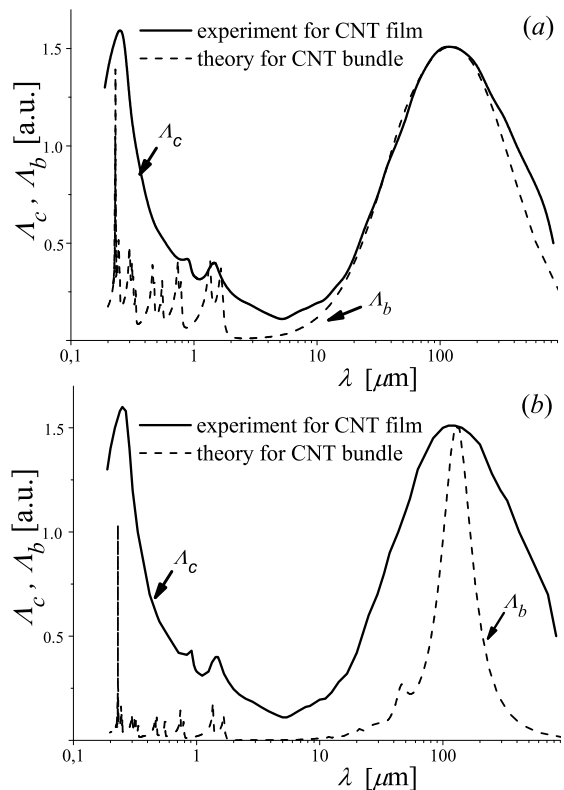


FIG. 2: Comparison between experimentally observed normalized absorbance  $\Lambda_c$  of single-walled CNT film, taken from Fig. 6 in Ref.<sup>34</sup>, and calculated normalized absorption cross-section  $\Lambda_b$  of CNT-bundle. The 1.2  $\mu\text{m}$  length CNT bundle consists of three zigzag tubes with chiral vectors (13,0), (12,0) and (11,0), respectively. In calculations we set  $\tau = 2.2 \times 10^{-14}$  s for plot (a) and  $\tau = 1 \times 10^{-13}$  s for plot (b).

surface wave in metallic (12,0) CNT, whereas the contribution of semiconductor CNTs in this frequency range is negligibly small. Position of the peak on the frequency axis is determined by the CNT length, while its width is dictated by the electron free-path time  $\tau$ . In figure 2(a) both parameters have been chosen to provide the best correlation with the experimental plot:  $L = 1.2 \mu\text{m}$  and  $\tau = 2.2 \times 10^{-14}$  s. The later parameter turned out to be very close to that in graphite.

As one can see, theoretical curve follows the main peculiarities of the experimental one. Of course, variation of number of CNTs in the bundle and their chiral vectors modifies positions of peaks and their intensities. However, overall picture of the phenomenon is kept unchanged permitting the use of the bundle absorption cross-section as a model of the absorption in composite film with CNT bundles embedded. The model allows a qualitative physical interpretation of experimental results. In particular, as conductivity of all CNTs has plasmon resonance in the ultraviolet range at  $\lambda_{p1} = c\pi\hbar/\gamma_0 = 230 \text{ nm}$  (for  $\gamma_0 = 2.7 \text{ eV}$ ), the dependence  $\Lambda_b(\lambda)$  also has a resonance at this wavelength. This resonance is well

defined in the experimental plot. Thus, the main conclusion which follows from the comparison is that the experimentally observed absorption peak<sup>32,33,34,35</sup>, laying below the range of interband transitions, can certainly be attributed to geometrical (antenna) resonances of constituting finite-length CNTs, inhomogeneously broadened due to size dispersion in composites. It should be emphasized that the problem of inhomogeneous broadening is critical for the correct quantitative interpretation of absorption experiments in realistic CNT-based composites and requires distinct serious analysis which is far beyond the scope of given paper.

Figure 2(b) shows the same absorbance of the composite film as in Fig. 2(a) (solid line) and normalized absorption cross-section of the same CNT bundle as in Fig. 2(a) but for the value  $\tau = 1 \times 10^{-13}$  s (dashed line). The picture illustrates strong dependence of the antenna peak linewidth of the CNT bundle on  $\tau$ .

### C. Near-zone field enhancement in finite-length CNT

Currently, there exists a considerable interest to optics of metal nanoparticles, largely due to their plasmonic properties<sup>53</sup> and ability to produce giant and highly localized electromagnetic fields<sup>54,55</sup>. Important applications include microscopy<sup>56</sup>, spectroscopy<sup>57</sup>, optoelectronic devices<sup>58</sup> and, as aforementioned, photothermolysis of living cells<sup>40,41,42</sup>. Naturally, one can expect manifestation of analogous effects in metallic CNTs. Since their conductivity in the infrared (terahertz) regime has Drude-like behavior, the propagation of surface waves along the CNT axis<sup>2</sup> is provided, which are analogous to plasmon-polariton wave in elongated metallic particles<sup>53</sup>. The surface wave propagation is accompanied by the field localization near the CNT edges. Further we discuss this effect on more details.

The spatial structure of electric field in the near zone is conveniently characterized by the intensity enhancement factor  $\xi(\mathbf{r}, \omega) = |\mathbf{E}(\mathbf{r}, \omega)|^2 / |\mathbf{E}^{(0)}|^2$ , where  $|\mathbf{E}(\mathbf{r}, \omega)|^2$  is electric field intensity distribution and  $|\mathbf{E}^{(0)}|^2$  is electric field intensity of incident plane-wave illumination. One can expect that in the vicinity of geometrical (antenna) resonance the spatial and frequency variables are separated to a high accuracy allowing the enhancement factor expression as

$$\xi(\mathbf{r}, \omega) \sim \frac{\varphi(\mathbf{r})}{(\omega - \omega_1)^2 + (\omega_1/2Q)^2}, \quad (13)$$

where  $\omega_1$  is the angular frequency corresponding to the first geometrical resonance,  $Q$  is  $Q$ -factor of the resonant mode, and  $\varphi(\mathbf{r})$  is a spatial distribution function.

The field intensity distribution near finite-length CNTs illuminated by a plane wave with the electric field vector directed along CNT axis is presented in Fig. 3. The incident wavelengths correspond to the first geometrical resonances of chosen CNTs. The constant-value

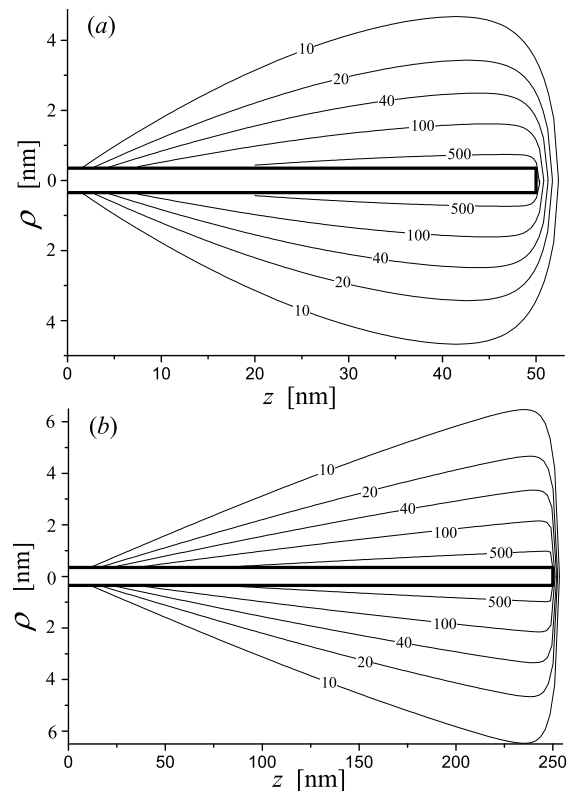


FIG. 3: The constant-value lines of the intensity enhancement factor  $\xi(\mathbf{r}, \omega_1)$  in the vicinity of the right half of (9,0) zigzag CNT with the radius  $R = 0.36$  nm and the length (a)  $L = 100$  nm, and (b)  $L = 500$  nm. In both cases  $\tau = 2 \times 10^{-14}$  s. CNT is shown by the thick line. The incident wavelength corresponds to the first antenna resonance: (a)  $\lambda_1 = 12.7 \mu\text{m}$  and (b)  $\lambda_1 = 57 \mu\text{m}$ .

lines of the intensity enhancement factor  $\xi(\mathbf{r}, \omega_1) \sim \varphi(\mathbf{r})$  are depicted. As the field distribution at resonance frequency is symmetrical with respect to the plane  $z = 0$ , i.e.  $\xi(\mathbf{r}, \omega_1) = \xi(-\mathbf{r}, \omega_1)$ , the right half of CNTs is only shown.

Figure 3 demonstrates considerable,  $\xi \sim 500$ , and increasing nearby edges the near-zone field enhancement. Such a spatial distribution of the field intensity is dictated by general principles of electrodynamics and can easily be understood from the absence of free charges at the CNT tips (mathematically they are geometrical singularities of the surface) resulting in the field localization near the tips<sup>51</sup>. The simplest example is a perfectly conducting semiinfinite plane described by the spatial distribution function  $\varphi(\mathbf{r}) \sim |\mathbf{r}|^{-1}$ ; here  $\mathbf{r}$  is the distance from the plane verge. In more realistic models the verge is described by strongly curved but regular functions<sup>51</sup>.

The intensity enhancement factor versus wavelength calculated in a fixed point  $\mathbf{r}_1$  at different  $\tau$  is depicted in Fig. 4. As one can see, maximum magnitude of  $\xi$  strongly increases with  $\tau$  and reaches e.g. 5000 for  $\tau = 1 \times 10^{-13}$  s, which corresponds to the electron mean free path  $\sim 100$

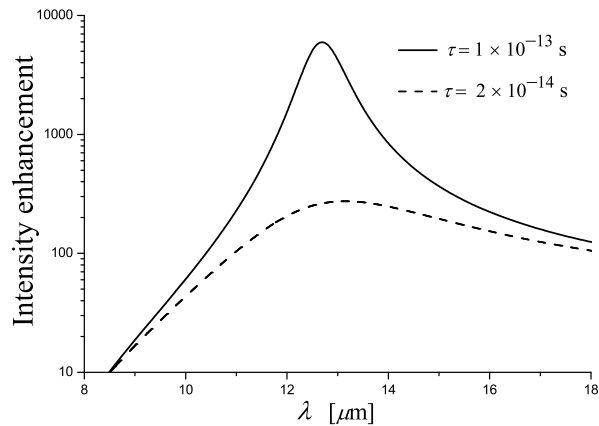


FIG. 4: The intensity enhancement factor  $\xi(\mathbf{r}_1, \lambda)$  vs wavelength for 100 nm length metallic zigzag (9,0) CNT at different magnitudes of the free-pass time:  $\tau = 1 \times 10^{-13}$  s (solid line), and  $\tau = 2 \times 10^{-14}$  s (dashed line). Calculation has been performed for the space point given by cylindrical coordinates  $\rho_1 = 1$  nm and  $z_1 = 47.5$  nm of the coordinate system presented in Fig 3(a).

nm. Experimental results indicate that  $\tau$  in single-walled CNTs in the regime of Drude conductivity can be much higher than in normal metal<sup>59</sup>. Thus, the intensity enhancement factor 5000 and even bigger is quite reachable.

It can easily be shown that in the vicinity of the antenna resonance  $\lambda_1 = 2\pi c/\omega_1$  the dependence  $\xi(\mathbf{r}_1, \lambda)$  depicted in Fig. 4 follows the Lorentz resonant line, supporting therefore our assumption resulted in Eq. (13). In the vicinity of resonance the enhancement factor is reduced to a product of two partial independent factors, one of which is completely determined by the geometrical singularities of the CNT at its tips, while the second one – by the frequency singularity due to antenna resonance. Note that the same structure of the field enhancement factor,  $L_{\text{pl}} = L_{LR}L_{SPPR}$ , has been revealed for rough surfaces of metals<sup>60</sup> and for metallic nanoparticles<sup>54,55</sup> in the vicinity of plasmon resonance (the field and the intensity enhancement factors,  $L_{\text{pl}}$  and  $\xi$  respectively, are related by  $L_{\text{pl}} = \sqrt{\xi}$ ).  $L_{LR}$  and  $L_{SPPR}$  are the partial factors denoting to the lightning rod effect<sup>55,60</sup> and plasmon resonance, correspondingly. Comparison shows that the lightning rod effect physically is identical to mechanism described for CNTs by the factor  $\varphi(\mathbf{r})$  ( $L_{LR} = \sqrt{\varphi(\mathbf{r})}$ ), whereas resonant coefficient in (13) corresponds to the factor  $L_{SPPR}$ : instead plasmons characteristic for metal particles, surface waves propagate in CNTs. The dif-

ference is that the field enhancement in metal particles is observed in the range of plasmon resonance, i.e. in the wavelength range 400 – 1300 nm, while the CNT antenna resonance at realistic CNT lengths occupied the far-IR and terahertz regions. The use of CNT bundles instead isolated CNTs shifts the operating range in the short-wavelength direction<sup>17</sup>.

#### IV. CONCLUSION

In the paper, we have modeled absorption cross-section and near-zone field enhancement in isolated single-wall carbon nanotubes in a wide spectral range – from terahertz to optical frequencies. Comparison with experiments on absorption properties of CNT-based composites allowed proposing a qualitative interpretation of observed peculiarity – resonant-like behavior of the absorbance below the range of interband transition. We state the peak to be due to geometrical (antenna) resonance of surface waves in finite-length CNTs. As the phase velocity  $v$  of surface wave in CNT is 50 – 100 times smaller than the speed of light in vacuum, the first geometrical resonance of this wave occurs for the tube length 50 – 100 times smaller than the incident wavelength. In other words, for typical CNT lengths 0.1 – 1  $\mu\text{m}$  the antenna resonance-induced peak is shifted into far-IR or terahertz region. Note that a hypothetical rod with bulk conductivity of gold and with radius below 0.5 nm is also characterized by a strong slowing down of plasmon-polariton mode<sup>54</sup> ( $c/v = 50 - 100$ ). However, fabrication of such thin metallic rods is technologically difficult problem. Another advantage of CNT comparing with metallic antenna is considerable time of electron mean free path in the regime of Drude conductivity, that likely leads to stronger field localization near CNT, than near the realistic metallic antenna. Therefore, CNTs look advantageous for systems operating in far-IR or terahertz regions, directed to both optoelectronic and biomedical applications.

#### Acknowledgments

The research was partially supported by the INTAS under projects 05-100008-7801 and 06-100013-9225, International Bureau BMBF (Germany) under project BLR 08/001, and the Belarus Republican Foundation for Fundamental Research and CNRS (France) under project F07F-013. M.V.S. acknowledges a support through the World Federation of Scientists fellowship.

<sup>1</sup> S. Reich, C. Thomsen, J. Maultzsch, Carbon Nanotubes. Basic Concepts and Physical Properties, Wiley-VCH, Berlin, (2004)

<sup>2</sup> G. Ya. Slepyan, S. A. Maksimenko, A. Lakhtakia, O. Yevtushenko, and A. V. Gusakov, *Phys. Rev. B.* 60, 17136

(1999)

<sup>3</sup> S. A. Maksimenko and G. Ya. Slepyan, Electrodynamic properties of carbon nanotubes, in *Electromagnetic Fields in Unconventional Materials and Structures*, edited by O. N. Singh and A. Lakhtakia, Wiley, New York, (2000), pp.

- 217-255.
- <sup>4</sup> J. Haggmann, *IEEE Trans. Nanotechnol.* 4, 289 (2005).
  - <sup>5</sup> J. Rybczynski, K. Kempa, A. Herczynski, Y. Wang, M. J. Naughton, Z. F. Ren, Z. P. Huang, D. Cai, M. Giersig, *Appl. Phys. Lett.* 90, 021104 (2007)
  - <sup>6</sup> A. Raychowdhury, and K. Roy, *IEEE Trans. Computer-Aided Design* 25, 58 (2006)
  - <sup>7</sup> G. Miano, F. Villone, *IEEE Trans. Antennas Propag.* 54, 2713 (2006)
  - <sup>8</sup> A. G. Chiariello and G. Miano, *COMPEL: Int. J. for Computations and Mathematics in Electrical and Electronic Engineering* 26, 571 (2007)
  - <sup>9</sup> A. Maffucci, G. Miano, F. Villone, *Int. J. Circuit Theory and Appl.* 36, 31 (2008)
  - <sup>10</sup> H. Li, W.-Y. Yin, K. Banerjee, and J.-F. Mao, *IEEE Trans. Electron Devices* 55, 1328 (2008)
  - <sup>11</sup> Y. Wang, K. Kempa, B. Kimball, G. Benham, W. Z. Li, T. Kempa, J. Rybczynski, A. Herczynski, and Z. F. Ren, *Appl. Phys. Lett.* 85, 2607 (2004)
  - <sup>12</sup> G. W. Hanson, *IEEE Trans. Antennas Propag.* 53, 3426 (2005)
  - <sup>13</sup> P. J. Burke, S. Li, and Z. Yu, *IEEE Trans. Nanotechnol.* 5, 314 (2006)
  - <sup>14</sup> G. Ya. Slepyan, M. V. Shuba, S. A. Maksimenko, and A. Lakhtakia, *Phys. Rev. B.* 73, 195416 (2006)
  - <sup>15</sup> J. Hao, and G. W. Hanson, *Phys. Rev. B.* 74, 035119 (2006)
  - <sup>16</sup> K. Kempa, J. Rybczynski, Z. Huang, K. Gregorczyk, A. Vidan, B. Kimball, J. Carlson, G. Benham, Y. Wang, A. Herczynski, Z. F. Ren, *Advanced Materials* 19, 421 (2007)
  - <sup>17</sup> M. V. Shuba, S. A. Maksimenko, and A. Lakhtakia, *Phys. Rev. B.* 76, 155407 (2007)
  - <sup>18</sup> A. M. Nemilentsau, G. Ya. Slepyan, S. A. Maksimenko, *Phys. Rev. Lett.* 99, 147403 (2007)
  - <sup>19</sup> Y. Wang, Q. Wu, W. Shi, X. He, X. Sun, T. Gui, *Int. J. Infrared Millim. Waves* 29, 35 (2008)
  - <sup>20</sup> G. W. Hanson, *IEEE Antennas Propag. Mag.*, to be published, (2008)
  - <sup>21</sup> S. A. Maksimenko, G. Ya. Slepyan, A. M. Nemilentsau, and M. V. Shuba, *Physica E.* 40, 2360 (2008)
  - <sup>22</sup> C. Rutherglen, and P. Burke, *Nano Lett.* 7, 3296 (2007)
  - <sup>23</sup> K. Iensen, I. Weldon, H. Garsia, and A. Zettl, *Nano Lett.* 7, 3508 (2007)
  - <sup>24</sup> J. A. Misewich, R. Martel, Ph. Avouris, J. C. Tsang, S. Heinze, J. Tersoff, *Science* 300, 783 (2003)
  - <sup>25</sup> J. Chen, V. Perebeinos, M. Freitag, J. Tsang, Q. Fu, J. Liu, and P. Avouris *Science* 310, 1171 (2005)
  - <sup>26</sup> O. V. Kibis, M. E. Portnoi, *Tech. Phys. Lett.* 31, 671 (2005)
  - <sup>27</sup> O. V. Kibis, M. Rosenau da Costa, and M. E. Portnoi, *Nano Lett.* 7, 3414 (2007)
  - <sup>28</sup> K. G. Batrakov, P. P. Kuzhir, S. A. Maksimenko, *Proc. SPIE* 6328, 63280Z (2006)
  - <sup>29</sup> P. Kuzhir, K. Batrakov, S. Maksimenko, *Synthesis and Reactivity in Inorganic, Metal-Organic and Nano-Metal Chemistry* 37, 341 (2007)
  - <sup>30</sup> K. G. Batrakov, P. P. Kuzhir, and S. A. Maksimenko, *Physica E.* 40, 1065 (2008)
  - <sup>31</sup> M. J. O'Connell, S. M. Bachilo, C. B. Huffman, V. C. Moore, M. S. Strano, E. H. Haroz, K. L. Rialon, P. J. Boul, W. H. Noon, C. Kittrell, J. Ma, R.H. Hauge, R. B. Weisman, R. E. Smalley, *Science* 297, 593 (2002)
  - <sup>32</sup> F. Bommeli, O. L. Degiorgi, P. Wachter, W. S. Bacsa, W. A. de Hee and L. Forro, *Solid State Commun.* 99, 513 (1996)
  - <sup>33</sup> A. Ugawa, A. G. Rinzler, and D. B. Tanner, *Phys. Rev. B.* 60, R11305 (1999)
  - <sup>34</sup> H. Hu, B. Zhao, M. A. Hamon, K. Kamaras, M. E. Itkis, R. C. Haddon, *J. Am. Chem. Soc.* 125, 14893 (2003)
  - <sup>35</sup> C. Kang, I. H. Maeng, S. J. Oh, S. C. Lim, K. H. An, Y. H. Lee, and J.-H. Son, *Phys. Rev. B.* 75, 085410 (2007)
  - <sup>36</sup> N. W. S. Kam, M. O'Connell, J. A. Wisdom, and H. Dai, *Proc. Natl. Acad. Sci. USA*, 102, 11600 (2005)
  - <sup>37</sup> B. Panchapakesan, S. Lu, K. Sivakumar, K. Teker, G. Cesarone, and E. Wickstrom, *NanoBiotechnology*, 1, 133 (2005)
  - <sup>38</sup> C. J. Gannon, P. Cherukuri, B. I Yakobson, L. Cognet, J. S Kanzius, C. Kittrell, R B. Weisman, M. Pasquali, H. K. Schmidt, R. E. Smalley, S. A Curley, *Cancer* 110, 2654 (2007)
  - <sup>39</sup> W. Yang, P. Thordarson, J. J. Gooding, S. P. Ringer and F. Braet, *Nanotechnology* 18, 412001 (2007)
  - <sup>40</sup> V. P. Zharov, E. N. Galitovskaya, C. Johnson, T. Kelly, *Lasers Surg. Med.* 37, 219 (2005)
  - <sup>41</sup> D. O. Lapotko, E. Y. Lukianova-Hleb, A. A. Oraevsky, *Nanomedicine* 2, 241 (2007)
  - <sup>42</sup> X. Huang, P. K. Jain, I. H. El-Sayed, and M. A. El-Sayed, *Lasers Med. Sci.* DOI: 10.1007/s10103-007-0470-x (2007)
  - <sup>43</sup> J. Gemmer, M. Michel and G. Mahler, *Quantum Thermodynamics: Emergence of Thermodynamic Behaviour within Composite Quantum Systems*, Lect. Notes Phys. 657, Springer, Berlin-Heidelberg, (2005).
  - <sup>44</sup> *Microscale and Nanoscale Heat Transfer*, Topics Appl. Phys. 107, edited by S. Volz, Springer, Berlin-Heidelberg, (2007).
  - <sup>45</sup> S. Berber, Y.-K. Kwon, D. Tomaneck, *Phys. Rev. Lett.* 84, 4613 (2000).
  - <sup>46</sup> J. Che, T. Cagin, W.A. Goddard III, *Nanotechnology* 11, 65 (2000).
  - <sup>47</sup> M. A. Kuroda, A. Congellaris, J.-P. Leburton, *Phys. Rev. Lett.* 95, 266803 (2000).
  - <sup>48</sup> E. Pop, D. Mann, Q. Wang, K. Goodson, and H. Dol, *Nanolett.* 6, 96 (2006)
  - <sup>49</sup> M. S. Dresselhaus , G. Dresselhaus , A. Jorio , A. G. Souza Filho, R. Saito, *Carbon* 40, 2043 (2002)
  - <sup>50</sup> C. L. Kane and E. J. Mele, *Phys. Rev. Lett.* 78, 1932 (1997)
  - <sup>51</sup> A. S. Ilyinsky, G. Ya. Slepyan, and A. Ya. Slepyan, *Propagation, scattering and dissipation of electromagnetic waves*, Peter Peregrinus, London, (1993)
  - <sup>52</sup> J. W. Mintmire, and C. T. White, *Phys. Rev. Lett.* 81, 2506 (1998)
  - <sup>53</sup> L. Novotny, and B. Hecht, *Principles of Nano-Optics*, Cambridge University Press, Cambridge, (2006)
  - <sup>54</sup> K. B. Crozier, A. Sundaramurthy, G. S. Kino, and C. F. Quate, *J. Appl. Phys.* 94, 4632 (2003)
  - <sup>55</sup> R. Kappeler, D. Erni, C. Xudong, and L. Novotny, *J. Comput. Theor. Nanoscience* 4, 686 (2007)
  - <sup>56</sup> J. T. Krug, E. J. Sanchez, and X. S. Xie, *J. Chem. Phys.* 116, 10895 (2002)
  - <sup>57</sup> R. Hillenbrand, T. Taubner, and F. Keilmann, *Nature* (London) 418, 159 (2002)
  - <sup>58</sup> I. Puscasu, D. Spencer, and G. D. Boreman, *Appl. Opt.* 39, 1570 (2000)
  - <sup>59</sup> O. Hilt, H. B. Brom, and M. Ahlskog, *Phys. Rev. B.* 61, R5129 (2000)
  - <sup>60</sup> G. T. Boyd, T. Rasing, J. R. R. Leite, Y. R. Shen, *Phys. Rev. B.* 30, 519 (1984)